Available online at www.sciencedirect.com
SCIENCE DIRECT®
Journal of Sound and Vibration 282 (2005) 617–634
JOURNAL OF SOUND AND VIBRATION
www.elsevier.com/locate/jsvi

Exact 3D piezoelasticity solution of hybrid cross–ply plates with damping under harmonic electro-mechanical loads

S. Kapuria[a,*], G.G.S. Achary[b]

[a]*Applied Mechanics Department, Indian Institute of Technology Delhi, Hauz Khas, New Delhi 110016, India*
[b]*ETD Department, Engineers India Limited, Bhikaji Cama Place, New Delhi 110066, India*

Received 14 July 2003; received in revised form 4 November 2003; accepted 2 March 2004
Available online 22 September 2004

Abstract

Three-dimensional (3D) piezoelasticity solution is presented for the steady-state forced response of simply supported hybrid cross-ply rectangular plates with embedded or surface-bonded piezoelectric layers under electromechanical harmonic excitation with damping. For each layer, all the entities are expanded in Fourier series to satisfy the boundary conditions at the edges. The governing equations reduce to ordinary differential equations in the thickness coordinate with constant coefficients. Their general solution is obtained using state-space technique. A transfer matrix approach is presented to obtain these from the electromechanical boundary conditions at the top and bottom of the plate, the conditions of prescribed potentials and the conditions of continuity/jump at the layer interfaces. Results for the amplitude and phase lag of the central deflection are presented for an elastic plate and for hybrid composite and sandwich plates. The reduction of deflection response by actuation of a piezoelectric layer is illustrated. The present benchmark solution would help assess 2D plate theories for damped response under harmonic loads.

1. Introduction

Composite laminates and sandwich structures with some embedded or surface-bonded piezoelectric layers, for sensing and actuation to achieve desired control, form part of a new

*Corresponding author. Tel.: +91-1126591218; fax: +91-1126581119.
E-mail address: kapuria@am.iitd.ernet.in (S. Kapuria).

0022-460X/$ - see front matter © 2004 Elsevier Ltd. All rights reserved.
doi:10.1016/j.jsv.2004.03.030

generation of smart adaptive structures. Accurate and efficient models are needed for response analysis of such hybrid piezoelectric plates. The exact three-dimensional (3D) solutions of rectangular laminated plates serve as useful benchmarks for the assessment of 2D plate theories and approximate 3D numerical solutions such as the solution using the finite element method. These exact solutions have provided insight into the complex coupled electromechanical behaviour of hybrid laminated plates and have led to the development of higher order 2D theories for plates. For laminated plates, layer-wise exact solutions of the governing field equations are obtained [1,2], and the arbitrary constants in the solutions are evaluated using the boundary conditions and the continuity and equilibrium conditions at the layer interfaces directly or indirectly by a layer-wise transfer matrix technique. The displacement or mixed formulation is used for the solution of the governing equations. Such 3D exact elasticity solutions for thick laminated rectangular elastic plates have been presented for static mechanical loading [1,2], thermal loading [3–5], free vibrations [1] and forced undamped vibrations [6]. 3D exact piezoelasticity solutions for rectangular hybrid piezoelectric plates have been presented for static electromechanical loading [7–15], thermal loading [16,17] and free vibrations [18,19]. Exact 2D piezoelasticity solution has been presented by Kapuria et al. [20] for steady-state forced response of hybrid piezoelectric beams using transfer matrices. To the authors' knowledge, exact elasticity and piezoelasticity solutions, for laminated elastic plates and hybrid piezoelectric plates with damping, under harmonic loads, are not available. Such solutions are needed to assess 2D hybrid plate theories since their error for the steady-state response is the cumulative error of the errors in predicting the static response, natural frequency and the dynamic magnification factor.

As exact closed form solutions can be obtained only for certain boundary conditions and loadings, so a simply supported rectangular plate under harmonic loading is chosen for analysis since an analytical closed form Fourier series solution can be obtained satisfying the boundary conditions at all its surfaces. This work presents an exact 3D piezoelasticity solution for the steady-state forced response of simply supported hybrid piezoelectric cross-ply rectangular plates with surface bonded or embedded piezoelectric layers, subjected to harmonic electromechanical loads with damping. The solution for laminated elastic composite and sandwich plates follows as a special case. The coupled piezoelectric constitutive equations, strain–displacement relations, field–gradient relations for electric displacements and electric potential, and the momentum and charge balance equations for the steady-state problem are solved exactly subject to the exact satisfaction of the boundary conditions at the top, bottom and the edge surfaces, and the continuity and equilibrium conditions at the layer interfaces. A mixed formulation is used for the governing field equations in terms of eight primary variables: displacements u, v, w, transverse stresses τ_{zx}, τ_{yz}, σ_z, electric potential ϕ and electric displacement D_z. For each layer, all the entities are expanded in double Fourier series that satisfy the boundary conditions at the four edge surfaces. The governing field equations reduce to eight first-order homogeneous differential equations in the thickness coordinate z with constant coefficients. Their general solution for each layer is obtained using state-space technique. For each layer, a transfer matrix relating the values of the eight primary variables at its bottom and its top is derived. The laminate transfer matrix relating the eight primary variables at the bottom and the top of the plate is built from the transfer matrices of the layers by using the continuity/jump conditions at the layer interfaces and the conditions of prescribed potentials at some layer interfaces. Numerical results for the amplitude

and phase lag of the central deflection are presented for highly inhomogeneous elastic test plate under harmonic pressure load, and for hybrid piezoelectric composite and sandwich plates under harmonic electromechanical loads. The reduction of the steady-state deflection response by actuation of a piezoelectric layer is illustrated. The benchmark solution presented herein would help assess the 3D numerical solutions and also assess 2D hybrid plate theories for the prediction of steady-state damped response under electromechanical harmonic loads.

2. Governing equations for 3D exact solution

Consider a hybrid rectangular plate (Fig. 1) having sides of length a and b along directions x and y, and total thickness h in direction z, subjected to harmonic electromechanical load. It is made of L perfectly bonded orthotropic layers which are stacked with two of their principal material directions along the sides of the rectangle. Some of the layers can be of piezoelectric material of orthorhombic class mm2 symmetry (commonly used PZT and PVDF belong to this class) with poling along the thickness axis z. The material of the piezoelectric layers can be different. The midplane of the plate is chosen as the xy-plane. The z-coordinate of the bottom surface of the kth layer (numbered from the bottom) is denoted as z_{k-1}. The thickness of the kth layer is $t^{(k)}$. The interface between the kth and the $(k+1)$th layer is named as the kth interface. The layer superscript is omitted unless needed for clarity. The sides of the plate at $x = 0$, a and $y = 0$, b are simply supported. The simply supported sides are idealized as supports which allow displacement normal to the boundary surface but prevent transverse tangential displacements.

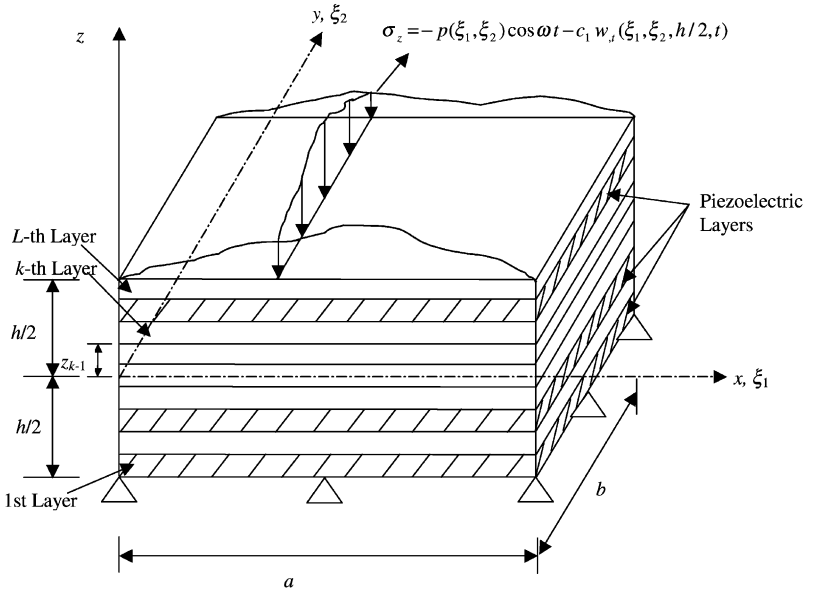

Fig. 1. Simply supported hybrid plate.

The strains $\varepsilon_x, \varepsilon_y, \varepsilon_z, \gamma_{yz}, \gamma_{zx}, \gamma_{xy}$ are related to the displacements u, v, w by

$$\varepsilon_x = u_{,x}, \quad \varepsilon_y = v_{,y}, \quad \varepsilon_z = w_{,z}, \tag{1}$$

$$\gamma_{yz} = v_{,z} + w_{,y}, \quad \gamma_{zx} = w_{,x} + u_{,z}, \quad \gamma_{xy} = u_{,y} + v_{,x}, \tag{2}$$

where a subscript comma denotes differentiation. The electric field components E_x, E_y, E_z are related to the electric potential ϕ by

$$E_x = -\phi_{,x}, \quad E_y = -\phi_{,y}, \quad E_z = -\phi_{,z}. \tag{3}$$

Using Eqs. (1)–(3), the 3D linear constitutive equations for the stresses $\sigma_x, \sigma_y, \sigma_z, \tau_{yz}, \tau_{zx}, \tau_{xy}$ and the electric displacements D_x, D_y, D_z, can be expressed as

$$u_{,x} = s_{11}\sigma_x + s_{12}\sigma_y + s_{13}\sigma_z - d_{31}\phi_{,z}, \tag{4}$$

$$v_{,y} = s_{12}\sigma_x + s_{22}\sigma_y + s_{23}\sigma_z - d_{32}\phi_{,z}, \tag{5}$$

$$w_{,z} = s_{13}\sigma_x + s_{23}\sigma_y + s_{33}\sigma_z - d_{33}\phi_{,z}, \tag{6}$$

$$v_{,z} + w_{,y} = s_{44}\tau_{yz} - d_{24}\phi_{,y}, \tag{7}$$

$$w_{,x} + u_{,z} = s_{55}\tau_{zx} - d_{15}\phi_{,x}, \tag{8}$$

$$u_{,y} + v_{,x} = s_{66}\tau_{xy}, \tag{9}$$

$$D_x = d_{15}\tau_{zx} - \varepsilon_{11}\phi_{,x}, \tag{10}$$

$$D_y = d_{24}\tau_{yz} - \varepsilon_{22}\phi_{,y}, \tag{11}$$

$$D_z = d_{31}\sigma_x + d_{32}\sigma_y + d_{33}\sigma_z - \varepsilon_{33}\phi_{,z}, \tag{12}$$

where $s_{ij}, d_{ij}, \varepsilon_{ij}$ are the elastic compliances, piezoelectric strain constants and the dielectric constants. The dynamic equations of momentum and charge balance without internal body force and charge source are

$$\sigma_{x,x} + \tau_{xy,y} + \tau_{zx,z} = \rho\ddot{u}, \tag{13}$$

$$\tau_{xy,x} + \sigma_{y,y} + \tau_{yz,z} = \rho\ddot{v}, \tag{14}$$

$$\tau_{zx,x} + \tau_{yz,y} + \sigma_{z,z} = \rho\ddot{w}, \tag{15}$$

$$D_{x,x} + D_{y,y} + D_{z,z} = 0. \tag{16}$$

where ρ is the mass density and the overdot represents differentiation with respect to time.

The dimensionless coordinates $\xi_1 = x/a$, $\xi_2 = y/b$, $\zeta^{(k)} = \left(z + h/2 - \sum_{i=1}^{k-1} t^{(i)}\right)/t^{(k)}$ are introduced for the kth layer. Let the harmonic forces per unit area applied on the bottom and top surfaces of the plate in direction z be $p_z^1 = 0$, $p_z^2 = -p(\xi_1, \xi_2)\cos\omega t$, where ω is the forcing frequency. Let there be distributed viscous resistance force with the distributed viscous damping coefficient of c_1 per unit area per unit transverse velocity of the top surface of the plate. Such a damping may model the viscous resistance force of the surrounding medium of the plate. At the

bottom and the top of the plate, let the prescribed harmonic potential ϕ or electric displacement D_z be $\psi_1(\xi_1,\xi_2)\cos\omega t$ and $\psi_2(\xi_1,\xi_2)\cos\omega t$ respectively. For actuation of surface bonded or embedded piezoelectric layers, let the number of layer interfaces whose potentials are prescribed be L_a with the qth prescribed potential being $\Phi_q(\xi_1,\xi_2)\cos\omega t$ for the interface n_q. Thus the boundary conditions for the simply supported plate with the four supporting sides grounded are

$$\text{at } \xi_1 = 0,1: \quad v = w = 0, \quad \sigma_x = 0, \quad \phi = 0, \tag{17}$$

$$\text{at } \xi_2 = 0,1: \quad u = w = 0, \quad \sigma_y = 0, \quad \phi = 0, \tag{18}$$

$$\text{at } z = -\tfrac{1}{2}h: \quad \tau_{zx} = \tau_{zy} = 0, \quad \sigma_z = 0, \quad \phi/D_z = \psi_1\cos\omega t, \tag{19}$$

$$\text{at } z = \tfrac{1}{2}h: \quad \tau_{zx} = \tau_{zy} = 0, \quad \sigma_z = -p\cos\omega t - c_1\dot{w}(\xi_1,\xi_2,h/2,t), \quad \phi/D_z = \psi_2\cos\omega t. \tag{20}$$

The conditions of prescribed potentials of interfaces can be expressed as

$$[\phi|_{\zeta=1}]^{(n_q)} = \Phi_q(\xi_1,\xi_2)\cos\omega t, \quad q = 1,\ldots,L_a. \tag{21}$$

The equilibrium and the compatibility conditions at the interface between adjacent layers are

$$[(u,v,w,\tau_{zx},\tau_{yz},\sigma_z,\phi,D_z)|_{\zeta=1}]^{(k)} = [(u,v,w,\tau_{zx},\tau_{yz},\sigma_z,\phi,D_z)|_{\zeta=0}]^{(k+1)} \tag{22}$$

for $k = 1,\ldots,L-1$, except for D_z at the interfaces $k = n_q$, $q = 1,\ldots,L_a$. The prescribed potential applied to the interface n_q, induces an extraneous surface charge density, say $\tau_q(\xi_1,\xi_2,t) = D_{z_l} - D_{z_u}$ on this surface where the subscripts u and l refer to the upper and the lower faces of the interface. Thus the conditions of discontinuity of D_z for the interfaces n_q are

$$[D_z|_{\zeta=1}]^{(n_q)} = [D_z|_{\zeta=0}]^{(n_q+1)} - \tau_q(\xi_1,\xi_2,t), \quad q = 1,\ldots,L_a. \tag{23}$$

A mixed formulation is used for the 3D governing equations for vibration, by expressing them in terms of the eight basic entities $u,v,w,\tau_{zx},\tau_{yz},\sigma_z,\phi,D_z$, which appear in the boundary and interface conditions (19)–(22). The remaining entities $\sigma_x,\sigma_y,\tau_{xy},D_x,D_y$ are expressed in terms of these basic entities. Substituting $\phi_{,z}$ from Eq. (12) into Eqs. (4) and (5) and solving for σ_x,σ_y yields

$$\begin{aligned}\sigma_x &= b_{11}u_{,x} + b_{12}v_{,y} + b_{16}\sigma_z + b_{18}D_z,\\ \sigma_y &= b_{21}u_{,x} + b_{22}v_{,y} + b_{26}\sigma_z + b_{28}D_z,\end{aligned} \tag{24}$$

where

$$\begin{aligned}&s'_{ij} = s_{ij} - \frac{d_{3i}d_{3j}}{\varepsilon_{33}}, \quad d'_{3i} = \frac{d_{3i}}{\varepsilon_{33}},\\ &b_{11} = s'_{22}\bar{s}, \quad b_{12} = -s'_{12}\bar{s}, \quad b_{21} = b_{12}, \quad b_{22} = s'_{11}\bar{s},\\ &b_{16} = (s'_{12}s'_{23} - s'_{22}s'_{13})\bar{s}, \quad b_{18} = (s'_{12}d'_{32} - s'_{22}d'_{31})\bar{s},\\ &b_{26} = (s'_{12}s'_{13} - s'_{11}s'_{23})\bar{s}, \quad b_{28} = (s'_{12}d'_{31} - s'_{11}d'_{32})\bar{s},\end{aligned} \tag{25}$$

with $\bar{s} = [s'_{11}s'_{22} - s'^2_{12}]^{-1}$. Substituting σ_x,σ_y from Eq. (24) and $\phi_{,z}$ from Eq. (12) into Eq. (6) yields

$$w_{,z} = b_{31}u_{,x} + b_{32}v_{,y} + b_{36}\sigma_z + b_{38}D_z, \tag{26}$$

where

$$b_{31} = -b_{16}, \quad b_{36} = s'_{13}b_{16} + s'_{23}b_{26} + s'_{33},$$
$$b_{32} = -b_{26}, \quad b_{38} = s'_{13}b_{18} + s'_{23}b_{28} + d'_{33}. \tag{27}$$

Using Eqs. (24) and (26), Eqs. (8),(7),(13)–(15),(12) and (16) can be expressed as

$$u_{,z} = -w_{,x} + s_{55}\tau_{zx} - d_{15}\phi_{,x}, \tag{28}$$

$$v_{,z} = -w_{,y} + s_{44}\tau_{yz} - d_{24}\phi_{,y}, \tag{29}$$

$$\tau_{zx,z} = \rho\ddot{u} - \left(b_{11}u_{,xx} + \frac{u_{,yy}}{s_{66}}\right) - \left(b_{12} + \frac{1}{s_{66}}\right)v_{,xy} - b_{16}\sigma_{z,x} - b_{18}D_{z,x}, \tag{30}$$

$$\tau_{yz,z} = \rho\ddot{v} - \left(b_{21} + \frac{1}{s_{66}}\right)u_{,xy} - \left(b_{22}v_{,yy} + \frac{v_{,xx}}{s_{66}}\right) - b_{26}\sigma_{z,y} - b_{28}D_{z,y}, \tag{31}$$

$$\sigma_{z,z} = \rho\ddot{w} - \tau_{zx,x} - \tau_{yz,y}, \tag{32}$$

$$\phi_{,z} = b_{71}u_{,x} + b_{72}v_{,y} + b_{76}\sigma_z + b_{78}D_z, \tag{33}$$

$$D_{z,z} = -d_{15}\tau_{zx,x} - d_{24}\tau_{yz,y} + \varepsilon_{11}\phi_{,xx} + \varepsilon_{22}\phi_{,yy}, \tag{34}$$

where

$$b_{71} = -b_{18}, \quad b_{76} = d'_{31}b_{16} + d'_{32}b_{26} + d'_{33},$$
$$b_{72} = -b_{28}, \quad b_{78} = d'_{31}b_{18} + d'_{32}b_{28} - \frac{1}{\varepsilon_{33}}. \tag{35}$$

3. General solution of 3D governing equations

The electromechanical loads are of the separable form $g(\xi_1, \xi_2)\cos\omega t = \mathrm{Re}[g(\xi_1, \xi_2)\mathrm{e}^{\mathrm{i}\omega t}]$, where Re(...) denotes the real part of the complex number (...). Thus all the entities are expressed as $\mathrm{Re}[f(\xi_1, \xi_2)\mathrm{e}^{\mathrm{i}\omega t}]$, where $f(\xi_1, \xi_2)$ may be complex. For the kth layer, the solution of the governing field equations, satisfying the boundary conditions (17) and (18), is taken in the form of the following Fourier series:

$$(u, \tau_{zx}, D_x) = \sum_{m=1}^{\infty}\sum_{n=1}^{\infty} \mathrm{Re}[(u, \tau_{zx}, D_x)_{mn}\mathrm{e}^{\mathrm{i}\omega t}]\cos m\pi\xi_1 \sin n\pi\xi_2,$$
$$(v, \tau_{yz}, D_y) = \sum_{m=1}^{\infty}\sum_{n=1}^{\infty} \mathrm{Re}[(v, \tau_{yz}, D_y)_{mn}\mathrm{e}^{\mathrm{i}\omega t}]\sin m\pi\xi_1 \cos n\pi\xi_2,$$
$$(w, \sigma_z, \phi, D_z, \sigma_x, \sigma_y, \tau_q) = \sum_{m=1}^{\infty}\sum_{n=1}^{\infty} \mathrm{Re}[(w, \sigma_z, \phi, D_z, \sigma_x, \sigma_y, \tau_q)_{mn}\mathrm{e}^{\mathrm{i}\omega t}]\sin m\pi\xi_1 \sin n\pi\xi_2,$$
$$\tau_{xy} = \sum_{m=1}^{\infty}\sum_{n=1}^{\infty} \mathrm{Re}[\tau_{xy_{mn}}\mathrm{e}^{\mathrm{i}\omega t}]\cos m\pi\xi_1 \cos n\pi\xi_2, \tag{36}$$

where f_{mn} denotes the (m,n)th coefficient of the Fourier series expansion of a function $f(\xi_1,\xi_2,t)$. In order to satisfy termwise conditions (19)–(21) on the lateral surfaces and the interfaces, the given electromechanical loading functions $p(\xi_1,\xi_2),\psi_i(\xi_1,\xi_2),\Phi_q(\xi_1,\xi_2)$ are similarly expanded in Fourier series as

$$(p,\psi_i,\Phi_q)=\sum_{m=1}^{\infty}\sum_{n=1}^{\infty}\mathrm{Re}[(p,\psi_i,\Phi_q)_{mn}\mathrm{e}^{\mathrm{i}\omega t}]\sin\, m\pi\xi_1\,\sin\, n\pi\xi_2. \tag{37}$$

Substitution of the expansions from Eq. (36) into the eight governing equations (26) and (28) to Eq. (34) yields the following first-order homogeneous differential equations for the (m,n)th Fourier components of the eight basic entities:

$$X=[u_{mn}\ v_{mn}\ w_{mn}\ \tau_{zx_{mn}}\ \tau_{yz_{mn}}\ \sigma_{z_{mn}}\ \phi_{mn}\ D_{z_{mn}}]^{\mathrm{T}}, \tag{38}$$

$$X_{,\zeta}=QX, \tag{39}$$

where Q is an 8×8 constant matrix. The non-zero elements of Q are

$$\begin{aligned}
&Q_{13}=-t\bar{m},\quad Q_{14}=ts_{55},\\
&Q_{17}=-t\bar{m}d_{15},\quad Q_{23}=-t\bar{n},\\
&Q_{25}=ts_{44},\quad Q_{27}=-t\bar{n}d_{24},\\
&Q_{31}=-t\bar{m}b_{31},\quad Q_{32}=-t\bar{n}b_{32},\\
&Q_{36}=tb_{36},\quad Q_{38}=tb_{38},\\
&Q_{41}=t\left(\bar{m}^2b_{11}+\tfrac{\bar{n}^2}{s_{66}}\right)-\rho\omega^2,\quad Q_{46}=-t\bar{m}b_{16},\\
&Q_{42}=t\bar{m}\bar{n}\left(b_{12}+\tfrac{1}{s_{66}}\right),\quad Q_{48}=-t\bar{m}b_{18},\\
&Q_{51}=t\bar{m}\bar{n}\left(b_{21}+\tfrac{1}{s_{66}}\right),\quad Q_{52}=t\left(\bar{n}^2b_{22}+\tfrac{\bar{m}^2}{s_{66}}\right)-\rho\omega^2,\\
&Q_{56}=-t\bar{n}b_{26},\quad Q_{58}=-t\bar{n}b_{28},\\
&Q_{63}=-\rho\omega^2,\quad Q_{64}=t\bar{m},\\
&Q_{71}=-t\bar{m}b_{71},\quad Q_{65}=t\bar{n},\\
&Q_{76}=tb_{76},\quad Q_{72}=-t\bar{n}b_{72},\\
&Q_{84}=t\bar{m}d_{15},\quad Q_{78}=tb_{78},\\
&Q_{87}=-t(\bar{m}^2\varepsilon_{11}+\bar{n}^2\varepsilon_{22}),\quad Q_{85}=t\bar{n}d_{24},
\end{aligned} \tag{40}$$

where $\bar{m}=m\pi$, $\bar{n}=n\pi$. Eq. (39) is the state equation of ζ-invariant linear system with X being the state vector and Q being the system matrix. Its solution can be obtained as

$$X(\zeta)=\mathrm{e}^{(Q\zeta)}X(0), \tag{41}$$

where $\mathrm{e}^{(Q\zeta)}$ is computed analytically using the method described in Ref. [21].

Transfer matrix approach is presented to obtain the steady-state response. For the kth layer, the values X_k^- of X at the top ($\zeta = 1^-$) can be related to the value X_{k-1}^+ of X at the bottom ($\zeta = 0^+$) of this layer by a transfer matrix T_k as

$$X_k^- = T_k X_{k-1}^+, \quad T_k = \mathrm{e}^{Q}. \tag{42}$$

The transfer matrix $\bar{T}_q$ for the layers between n_q and n_{q+1} is obtained by applying Eqs. (42) successively to layers $n_q + 1$ to n_{q+1} and multiplying them. Using the continuity of X (Eq. (22)) at all the interfaces between the n_qth and the n_{q+1}th interface yields

$$X_{n_{q+1}}^- = \bar{T}_q X_{nq}^+, \quad \bar{T}_q = \prod_{j=n_q+1}^{n_q+1} T_j. \tag{43}$$

The product $\prod$ in Eq. (43) is taken from the right to the left. Eq. (43) is valid for $q = 0, 1, \ldots, L_a$ with $n_0 = 0$ and $n_{L_a+1} = L$. The discontinuity in D_z by τ_q in Eq. (23) at the interface n_q implies that X_{nq}^+ and X_{nq}^- are related by

$$X_{nq}^+ = X_{nq}^- + [0\ 0\ 0\ 0\ 0\ 0\ 0\ 1]^{\mathrm{T}} \tau_{qmn}. \tag{44}$$

Using Eqs. (43) and (44), X_{nq}^- and $X_0^+ = X_0$ are related by

$$X_{nq}^- = \prod_{i=0}^{q-1} \bar{T}_i X_0 + \sum_{p=1}^{q-1} \left(\prod_{k=p}^{q-1} \bar{T}_k [0\ 0\ 0\ 0\ 0\ 0\ 0\ 1]^{\mathrm{T}} \right) \tau_{pmn} = \hat{T}^q X_0 + \tilde{T}^q \tau, \tag{45}$$

where

$$\begin{aligned} &\hat{T}^q = \prod_{i=0}^{q-1} \bar{T}_i, \quad \tau = [\tau_1\ \tau_2 \ldots\ \tau_{L_a}]_{mn}^{\mathrm{T}}, \\ &\tilde{T}_{lj}^q = \left[\prod_{k=j}^{q-1} \bar{T}_k \right]_{l8}, \quad l = 1, 2, \ldots, 8;\ j = 1, \ldots, q-1; \\ &\tilde{T}_{lj}^q = 0, \quad l = 1, 2, \ldots, 8;\ j = q, \ldots, L_a. \end{aligned} \tag{46}$$

$\hat{T}^q$ is a 8×8 matrix and $\tilde{T}^q$ is a $8 \times L_a$ matrix. $X_L = X_L^- = X_{n_{L_a+1}}^-$ is obtained from Eq. (45) for $L = n_{L_a+1}$ as

$$X_L = \hat{T}^{L_a+1} X_0 + \tilde{T}^{L_a+1} \tau. \tag{47}$$

The interface conditions of Eq. (21) can be expressed as

$$\begin{aligned} &\Phi_{qmn} = (X_{nq}^-)_7 = \sum_{k=1}^{8} \hat{T}_{7k}^q X_{0_k} + \sum_{p=1}^{L_a} \hat{T}_{7p}^q \tau_{pn}, \quad q = 1, 2, \ldots, L_a \\ &\Rightarrow\ \Phi = \hat{T}_7 X_0 + \tilde{T}_7 \tau, \end{aligned} \tag{48}$$

where

$$\Phi = [\,\Phi_1 \quad \Phi_2 \quad \ldots \quad \Phi_{L_a}\,]^{\mathrm{T}}_{mn},$$
$$(\hat{T}_7)_{qk} = \hat{T}^q_{7k}, \quad (\tilde{T}_7)_{qp} = \tilde{T}^q_{7p}, \quad q,p = 1,\ldots,L_a,\ k = 1,\ldots,8. \tag{49}$$

$\hat{T}_7$ is a $L_a \times 8$ matrix and $\tilde{T}_7$ is a $L_a \times L_a$ matrix, τ is solved from Eq. (48) and substituted in Eq. (47) to yield the transfer matrix relation for X_L and X_0:

$$\tau = \tilde{T}_7^{-1}(\Phi - \hat{T}_7 X_0), \tag{50}$$

$$X_L = (\hat{T}^{L_a+1} - \tilde{T}^{L_a+1}\tilde{T}_7^{-1}\hat{T}_7)X_0 + \tilde{T}^{L_a+1}\tilde{T}_7^{-1}\Phi. \tag{51}$$

In X_0 and X_L, the seven known values from Eqs. (19) and Eq. (20) are

$$\begin{aligned} &X_{0_4} = (\tau_{zx_{mn}})_0 = 0, \quad X_{0_5} = (\tau_{yz_{mn}})_0 = 0,\\ &X_{0_6} = (\sigma_{z_{mn}})_0 = 0, \quad X_{0_7} = (\phi_{mn})_0 = \psi_{1_{mn}},\\ &X_{L_4} = (\tau_{zx_{mn}})_L = 0, \quad X_{L_5} = (\tau_{yz_{mn}})_L = 0,\\ &X_{L_7} = (\phi_{mn})_L = \psi_{2_{mn}}. \end{aligned} \tag{52}$$

The remaining nine primary unknowns at the bottom and the top are related by eight equations (51) and relation $(20)_2$ for the applied normal traction on the top surface

$$X_{L_6} = (\sigma_{z_{mn}})_L = -p_{mn} - \mathrm{i}\omega c_1 X_{L_3}. \tag{53}$$

These complex unknowns are determined from these nine algebraic equations. τ is then obtained using Eq. (50). For the undamped case, the unknowns are real as the imaginary term is zero on the right-hand side of Eq. (53). For the damped case, the magnitude and phase of the amplitude of an entity is given by the magnitude and the polar angle of the complex number representing it. All $X^{\pm}_{n_q}$ are thus obtained from Eqs. (45) and (44). For an interface k other than n_q, using continuity conditions (22) and Eq. (42) yield

$$X^+_k = X^-_k = \prod_{j=n_r+1}^{k} T_j X_{n_r}, \tag{54}$$

where n_r is the largest value of n_q, $q = 1,\ldots,L_a$ which is less than k. X at any ζ within a layer is finally obtained using Eq. (41). The stresses and electric displacements $\sigma_{x_{mn}}, \sigma_{y_{mn}}, \tau_{xy_{mn}}, D_{x_{mn}}, D_{y_{mn}}$ are then obtained using Eqs. (24) and Eqs. (9) to Eqs. (11). A procedure akin to the one described here, using transfer matrices, can be followed for the case when potential differences across some layers are also prescribed.

In the transfer matrix approach, the basic unknowns are only 9 which are independent of the number of layers. In contrast, if all conditions (19)–(22) are imposed directly without using transfer matrices, then the number of unknowns is $8L + L_a$ which depends on the number of layers. For $L = 6$, $L_a = 4$, the number of equations to be solved using these methods are 9 and 52, respectively.

For undamped synchronous free oscillations, at natural frequency ω_{mn}, for the (m,n)th Fourier component, Eq. (53) yields $X_{L_6}=0$. The homogeneous algebraic equations for the 8 unknowns are obtained from Eqs. (51). Their coefficient matrix depends on $\omega=\omega_{mn}$. For non-trivial solution, its determinant is zero, ω is incremented in small steps, monitoring sign changes in the determinant of the coefficient matrix and the value $\omega=\omega_{mn}$ is determined by the bisection method for which the determinant becomes zero.

4. Numerical results

Three highly inhomogeneous simply supported plates (a), (b) and (c) are analysed. The stacking order is mentioned from the bottom. The 6-ply elastic plate (a) has plys of thickness $0.1h/0.15h/0.25h/0.25h/0.15h/0.1h$ of materials 1/3/2/2/3/1 with orientations θ_k as $[0^\circ/0^\circ/90^\circ/0^\circ/0^\circ/0^\circ]$. It is a good test case since the plys have highly inhomogeneous stiffness in tension and shear. Plates (b) and (c) are hybrid plates consisting of an elastic substrate with two PZT-5A layers, each of thickness $0.1h$, with poling in $+z$ direction, bonded to the top and the bottom of the substrate. Plate (b) has a substrate of graphite–epoxy composite of material 4 with four plys of equal thickness $.2h$ having symmetric lay-up $[0^\circ/90^\circ/90^\circ/0^\circ]$. The substrate of plate (c) is a 5-layer sandwich construction with composite faces $[0^\circ/90^\circ]$ and a soft core with thicknesses $0.04h/0.04h/0.64h/0.04h/0.04h$. The interfaces between the substrate and the piezoelectric layers for the hybrid plates are grounded.

The material properties [22,23] are: $[(Y_1, Y_2, Y_3, G_{12}, G_{23}, G_{31}), \nu_{12}, \nu_{13}, \nu_{23}] =$

Material 1: [(6.9,6.9,6.9,1.38,1.38,1.38) GPa, 0.25,0.25,0.25]
Material 2: [(224.25,6.9,6.9,56.58,1.38,56.58) GPa, 0.25,0.25,0.25]
Material 3: [(172.5,6.9,6.9,3.45,1.38,3.45) GPa,0.25,0.25,0.25]
Material 4: [(181,10.3,10.3,7.17,2.87,7.17) GPa,0.28,0.28,0.33]
Face: [(131.1,6.9,6.9,3.588,2.3322,3.088) GPa, 0.32,0.32,0.49]
Core: [(0.2208,0.2001,2760,16.56,455.4,545.1) MPa, $0.99,3\times10^{-5},3\times10^{-5}$]
PZT-5A: [(61.0,61.0,53.2,22.6,21.1,21.1) GPa, 0.35,0.38,0.38], and $[(d_{31},d_{32},d_{33},d_{15},d_{24}),$
$(\eta_{11},\eta_{22},\eta_{33})] = [(-171,-171,374,584,584)\times10^{-12}\mathrm{m/V},(1.53,1.53,1.5)\times10^{-8}\mathrm{F/m}]$.

The density of materials 1,2,3,4 is $1578\,\mathrm{kg/m^3}$ and of PZT-5A, face and core is 7600,1000, $70\,\mathrm{kg/m^3}$, respectively. The dimensionless undamped natural frequency $\bar{\omega}_1=\omega_1 a S^2(\rho_0/Y_0)^{1/2}$

Table 1
Fundamental natural flexural frequency $\bar{\omega}_1$ for square and rectangular plates

S	Plate (a)		Plate (b)		Plate (c)	
	$b/a=1$	$b/a=2$	$b/a=1$	$b/a=4$	$b/a=1$	$b/a=4$
5	8.34453	6.94926	7.18099	4.89225	4.33615	2.58118
10	10.6797	8.90958	9.36860	6.44730	7.33896	4.80865

for the first bending mode is presented in Table 1 for the three plates with the top surface grounded and the bottom surface at charge free condition ($D_z = 0$). Two load cases are considered.

1. Pressure $p = -p_0 \sin(\pi x/a)\sin(\pi y/b)$ on the top surface with the potential $\psi_2 = 0$ and the electric displacement $\psi_1 = 0$ at the bottom surface. Thus the bottom piezoelectric layer acts as a sensory layer.
2. The actuation potential $\psi_2 = \phi_0 \sin(\pi x/a)\sin(\pi y/b)$ is applied to the top surface, the electric displacement $\psi_1 = 0$ at the bottom surface.

The results for these cases are non-dimensionalised with $S = a/h$, $Y_0 = 6.9\,\text{GPa}$ for plates (a) and (c) and $Y_0 = 10.3\,\text{GPa}$ for plate (b), $d_0 = 374 \times 10^{-12}\text{CN}^{-1}$. $\rho_0 = 1000\,\text{kg/m}^3$ for plate (c)

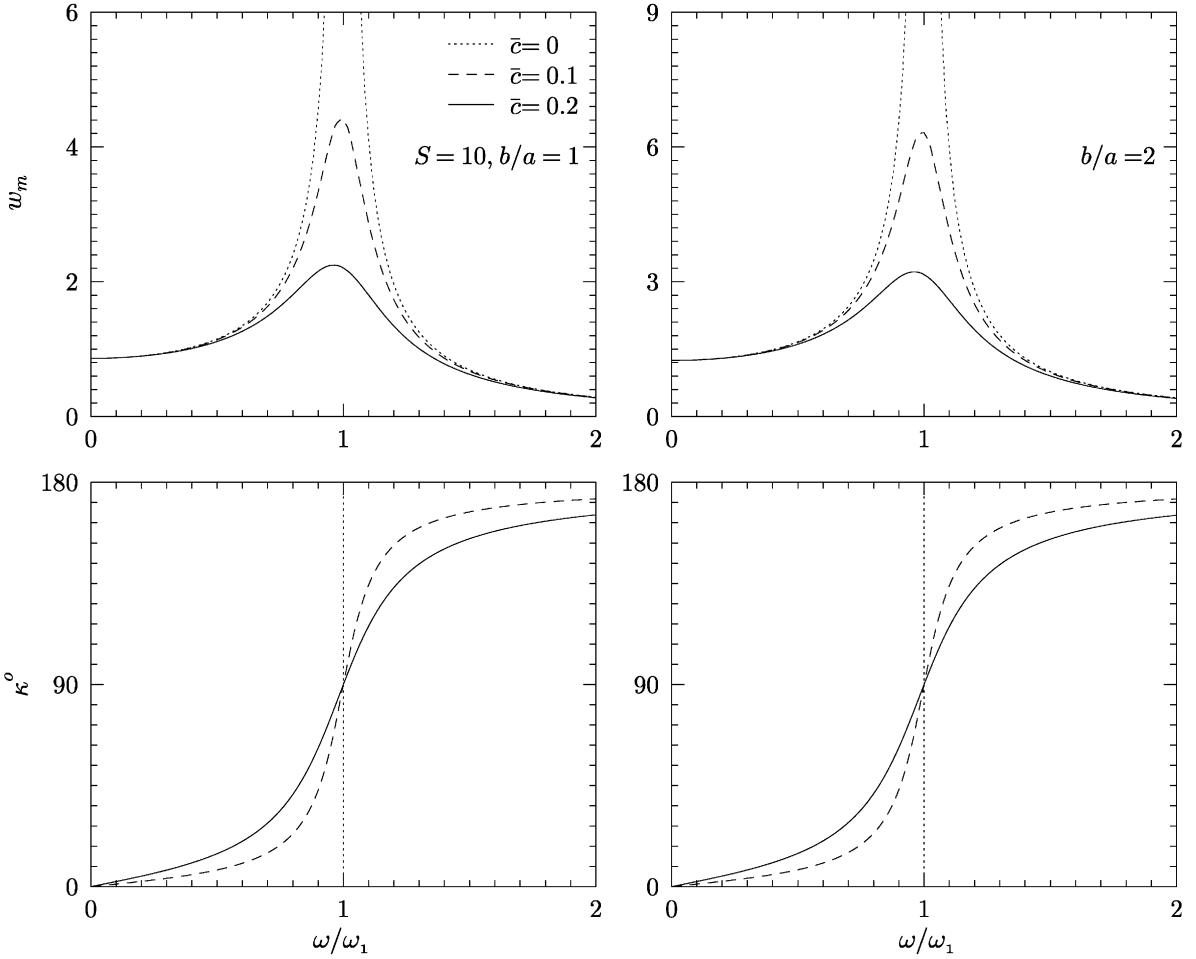

Fig. 2. Amplitude w_m and phase κ for square and rectangular plates (a) under load case 1.

and $\rho_0 = 1578\,\mathrm{kg/m^3}$ for the other plates:

1. $(\bar{u}, \bar{v}, \bar{w}) = 100(u, v, w/S)\,Y_0/hS^3p_0,\ (\bar{\sigma}_x, \bar{\sigma}_y) = (\sigma_x, \sigma_y)/S^2p_0,\ \bar{\phi} = 10^4\phi\,Y_0d_0/hS^2p_0,$
2. $(\tilde{u}, \tilde{v}, \tilde{w}) = (u, v, w/S)Sd_0\phi_0,\ (\tilde{\sigma}_x, \tilde{\sigma}_y) = (\sigma_x, \sigma_y)h/S^2\,Y_0d_0\phi_0,$

The damping parameter $\bar{c}$ is defined as $\bar{c} = c_1S/2\rho_0a\omega_1$.

The dimensionless amplitude w_m and phase lag κ of the midsurface deflection at the centre of the elastic composite plate (a) with aspect ratio $b/a = 1, 2$ and $S = 10$ are in plotted Fig. 2 as a function of ω/ω_1 for the pressure load case 1 for undamped case and for damped case with two values of damping, $\bar{c} = 0.1, 0.2$. Similar response curves for square hybrid plate (b) with composite substrate and plate (c) with sandwich substrate with $S = 10$ are shown in Figs. 3 and 4 for load cases 1 and 2. The pattern of these response curves for the moderately thick plates for the lightly damped cases considered herein is very much similar to those for a single-degree-of-freedom

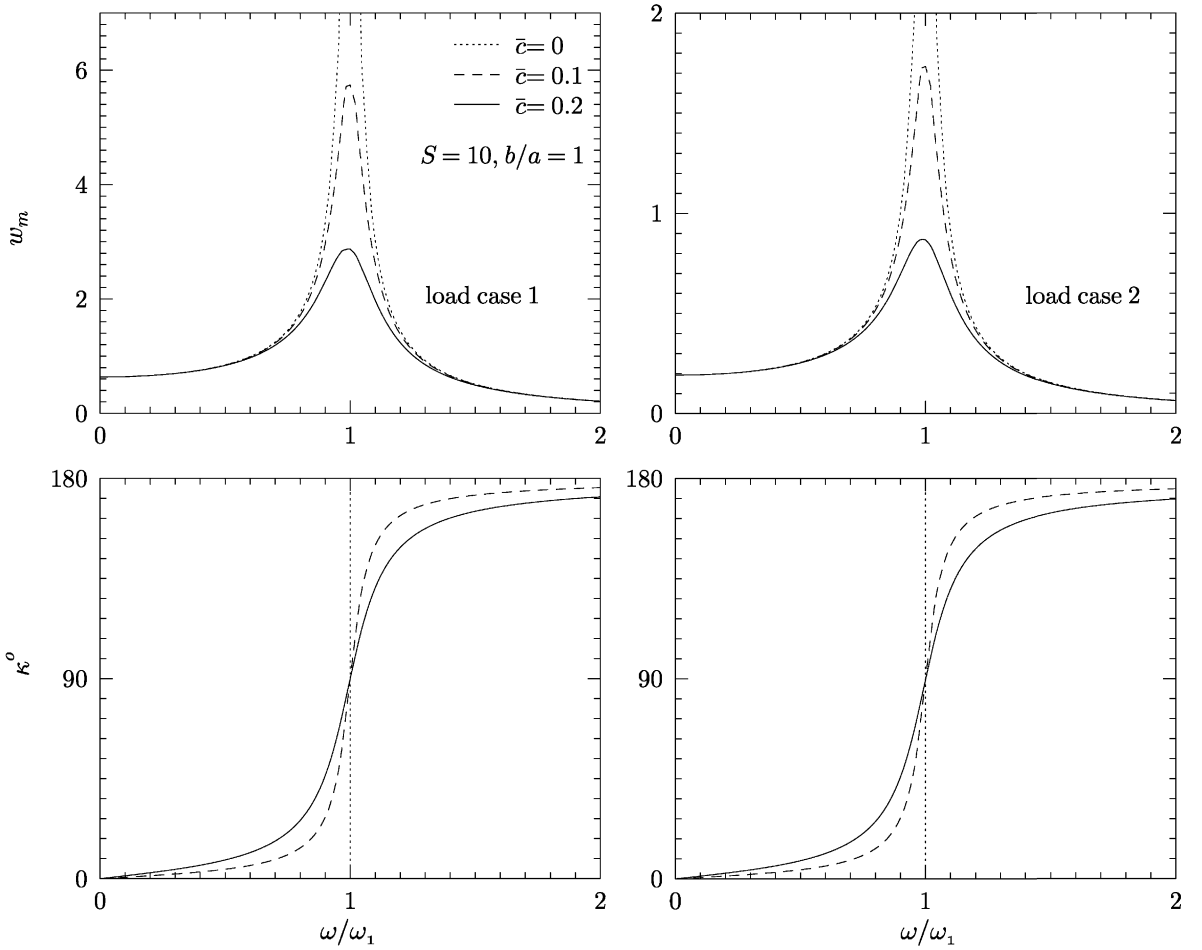

Fig. 3. Amplitude w_m and phase κ for square hybrid plate (b) under load cases 1 and 2.

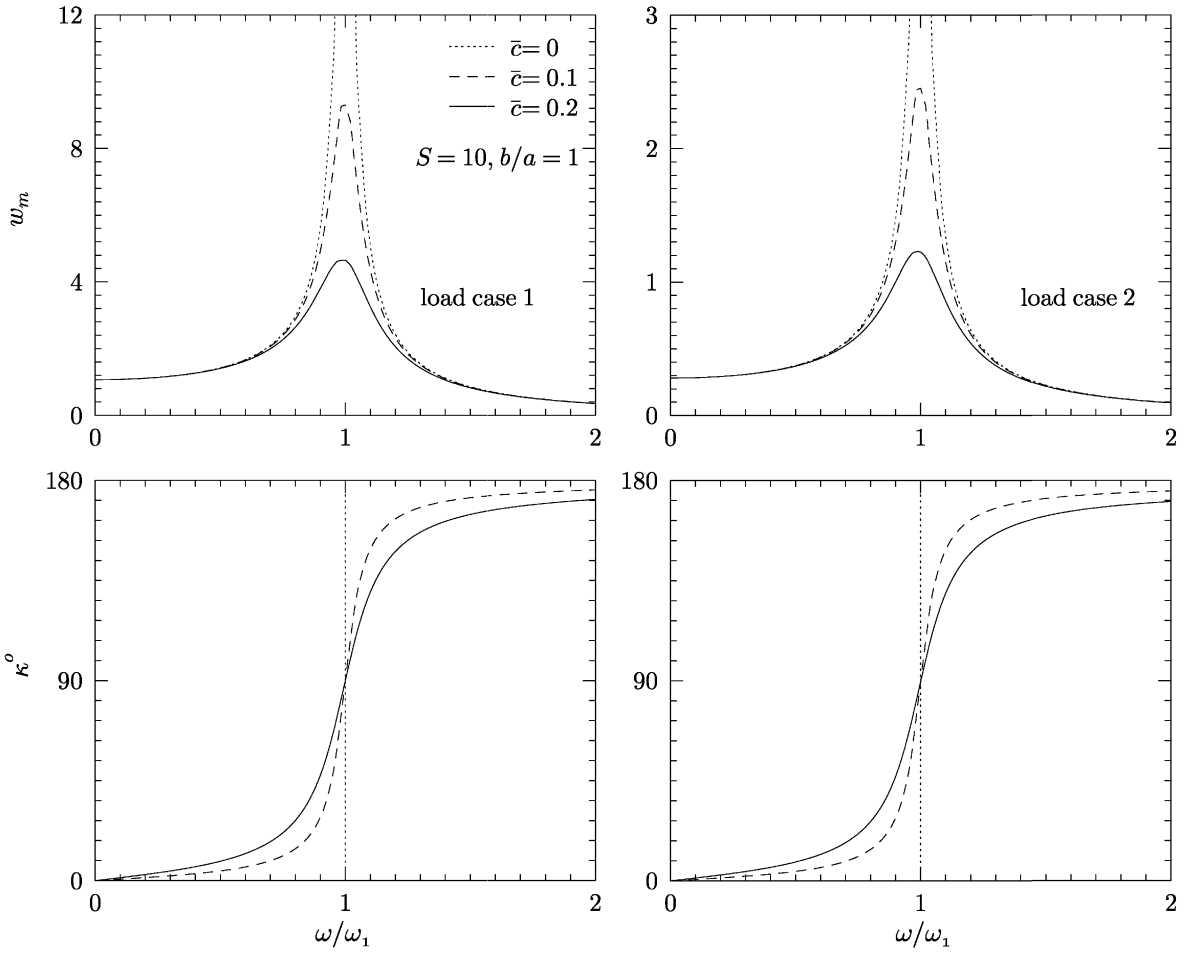

Fig. 4. Amplitude w_m and phase κ for square hybrid plate (c) under load cases 1 and 2.

system. The dimensionless values of amplitude w_m of central deflection and its phase lag κ for two values of $S, \omega/\omega_1$ and b/a of the three plates are given in Tables 2 and 3 for undamped and two lightly damped cases for load cases 1 and 2, respectively. The phase lag for the pressure load case 1 for hybrid plates is $\pi/2$ for $\omega/\omega_1 = 1$ for all values of $\bar{c}$ except for the thick sandwich plate (c) with $S = 5$, where κ differs from $\pi/2$ substantially. This difference increases with b/a and decreases with the damping. Similar observation can also be made for the potential load case 2 for sandwich plate (c). However, for load case 2, unlike the single-degree-of-freedom system, the phase lag for $\omega/\omega_1 = 1$ is found to differ marginally from $\pi/2$ for plate (b) also. This deviation is due to the coupling of bending and extensional modes which occurs in thick hybrid sandwich plates for both pressure and potential loads and in hybrid composite plates for potential load.

The through-the-thickness distributions of the amplitude of dimensionless deflection and predominant inplane displacement and normal stress for square hybrid plates (b) and (c) under load

Table 2
Amplitude and phase of central deflection of plates under load case 1

Plate	b/a	S	$w/w_1 = 0.7$					$w/w_1 = 1$			
			$\bar{c} = 0$	$\bar{c} = 0.1$		$\bar{c} = 0.2$		$\bar{c} = 0.1$		$\bar{c} = 0.2$	
			ω_m	ω_m	κ^0	ω_m	κ^0	ω_m	κ^0	ω_m	κ^0
(a)	1	5	2.7105	2.6194	14.90	2.3929	28.02	7.2806	90.00	3.6403	90.00
		10	1.6936	1.6353	15.08	1.4909	28.32	4.4091	90.00	2.2046	90.00
	2	5	3.9771	3.8389	15.15	3.4974	28.43	10.427	90.00	5.2136	90.00
		10	2.4499	2.3641	15.21	2.1524	28.53	6.3176	90.00	3.1588	90.00
(b)	1	5	2.0779	2.0546	8.58	1.9893	16.78	9.8267	90.00	4.9133	90.00
		10	1.2444	1.2302	8.64	1.1906	16.91	5.7409	90.00	2.8705	90.00
	4	5	4.5533	4.5011	8.69	4.3545	16.99	21.035	90.00	10.517	90.00
		10	2.6498	2.6191	8.74	2.5328	17.09	12.078	90.00	6.0389	90.00
(c)	1	5	5.0719	5.0257	7.75	4.8941	15.22	20.957	52.48	12.333	69.00
		10	2.0915	2.0660	8.96	1.9946	17.51	9.3013	90.00	4.6507	90.00
	4	5	8.4375	8.4110	4.54	8.3331	9.02	16.466	12.74	15.383	24.33
		10	4.8806	4.8209	8.97	4.6541	17.52	21.662	90.00	10.831	90.00

Table 3
Amplitude and phase of central deflection of plates under load case 2

Plate	b/a	S	$w/w_1 = 0.7$					$w/w_1 = 1$			
			$\bar{c} = 0$	$\bar{c} = 0.1$		$\bar{c} = 0.2$		$\bar{c} = 0.1$		$\bar{c} = 0.2$	
			ω_m	ω_m	κ^0	ω_m	κ^0	ω_m	κ^0	ω_m	κ^0
(b)	1	5	0.4190	0.4143	7.86	0.4012	15.35	1.9804	88.97	0.9907	87.94
		10	0.3761	0.3718	8.48	0.3598	16.58	1.7343	89.76	0.8672	89.52
	4	5	0.4963	0.4906	8.18	0.4747	15.98	2.2859	89.27	1.1432	88.55
		10	0.4241	0.4192	8.61	0.4054	16.82	1.9314	89.81	0.9657	89.62
(d)	1	5	0.5812	0.5759	7.19	0.5609	14.10	2.3857	51.68	1.4044	67.38
		10	0.5509	0.5442	8.81	0.5254	17.20	2.4520	89.78	1.2260	89.56
	4	5	0.7357	0.7333	4.31	0.7266	8.56	1.4334	12.40	1.3392	23.66
		10	0.8779	0.8671	8.89	0.8371	17.35	3.8986	89.88	1.9493	89.76

cases 1 and 2, are shown in Figs. 5 and 6 for $\omega/\omega_1 = 1$, $\bar{c} = 0.1$. It can be seen from Fig. 5 that the through-the-thickness distributions of w for the hybrid composite plate (b) is non-uniform especially across the piezolayers. The inplane displacement has a typical zigzag distribution across the thickness with strong discontinuities of slope at the interfaces with the piezolayers. These effects increase with the decrease in S. Moreover, the non-uniformity in the transverse displacement and the nonlinearity in the inplane displacement are more pronounced for the

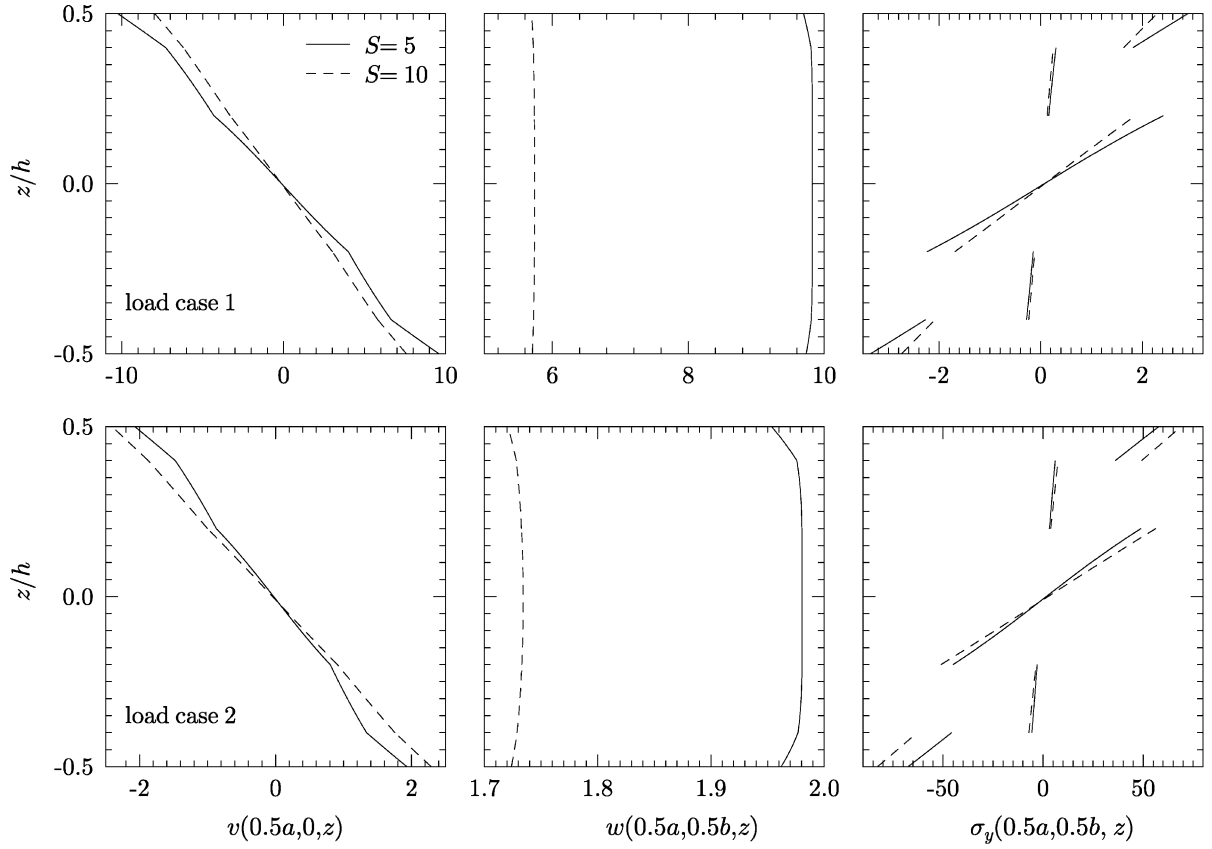

Fig. 5. Distributions of dimensionless amplitudes of v, w, σ_y for square hybrid plate (b) for $\omega/\omega_1 = 1$, $\bar{c} = 0.1$.

potential load case 2. The distribution of the inplane stresses becomes nonlinear across some layers for thick plates with $S = 5$. For sandwich plate (c), the inplane displacement has a zigzag distribution with large slope discontinuity at the interfaces with the core, even for a moderately thick plate with $S = 10$, for both the load cases 1 and 2. The non-uniformity in the distribution of w across the thickness increases with the decrease in S and is much more pronounced for the potential load case 2 compared to the pressure load case 1. In view of the above observations, it can be concluded that a smeared plate theory with a global through-the-thickness approximation of the displacement field would be inadequate to model accurately the steady state response of hybrid plates under electromechanical loads. A zigzag theory will be more appropriate to study such response of hybrid plates.

The effect of application of harmonic actuation potential of load case 2, on the steady-state amplitude $\bar{w}_m$ and phase lag κ of deflection at the centre of the hybrid plate (b) under harmonic pressure p_0 of load case 1, is shown in Fig. 7 for $S = 10$, $\bar{c} = 0.1$. For a given actuation potential $\bar{\phi}_0$, the percentage reduction in $\bar{w}_m$ is almost the same for wide range of ω/ω_1 since the $\bar{w}_m$ response curves for the two load cases are qualitatively similar.

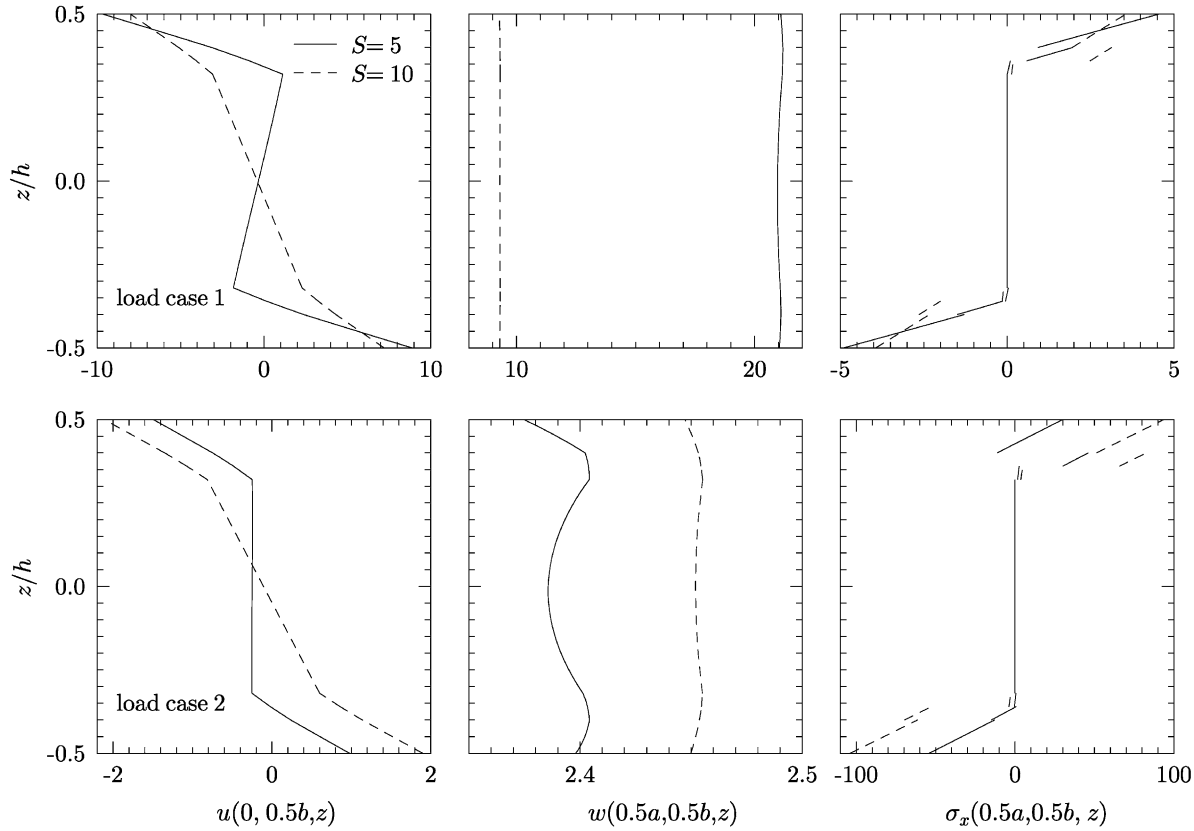

Fig. 6. Distributions of dimensionless amplitudes of u, w, σ_x for square hybrid plate (c) for $\omega/\omega_1 = 1$, $\bar{c} = 0.1$.

5. Conclusions

A benchmark 3D piezoelasticity exact solution is presented using transfer matrix approach, for simply supported hybrid piezoelectric plates with damping under electromechanical harmonic loads. The solution includes the cases wherein potential can be applied at any interface with the piezoelectric layers whether embedded or surface bonded. The exact deflection amplitude response curves follow the pattern of single-degree-of-freedom system. The benchmark numerical results presented herein, for elastic composite test plate and hybrid plates with composite and sandwich substrates would be useful to assess 2D theories of elastic and hybrid plates. The non-uniform distribution of deflection and the zigzag distributions of inplane displacements across the thickness imply that a smeared plate theory with a global through-the-thickness approximation of the displacement field would be inadequate to model accurately the steady state response of hybrid plates under electromechanical loads. A zigzag theory will be more appropriate to study such response of hybrid plates. Application of a passive harmonic actuation potential, for the harmonic pressure load case, results in

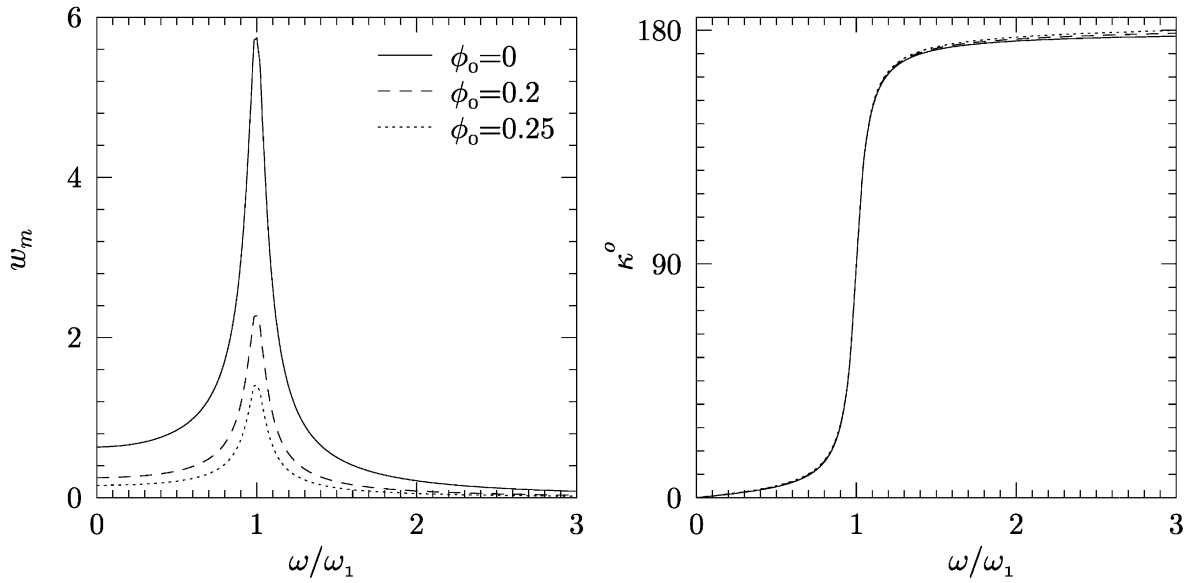

Fig. 7. Amplitude $\bar{w}_m$ and phase κ of hybrid square plate (b) under harmonic pressure with actuation potential.

almost the same percentage reduction of the amplitude of deflection for a large range of forcing frequency.

References

[1] S. Srinivas, A.K. Rao, Bending, vibration and buckling of simply supported thick-rectangular plates and laminates, *International Journal of Solids and Structures* 6 (1970) 1463–1481.
[2] N.J. Pagano, Exact solutions for rectangular bi-directional composite and sandwich plates, *Journal of Composite Materials* 4 (1970) 20–34.
[3] S. Srinivas, A.K. Rao, A note on flexure of thick rectangular plates and laminates with variation of temperature across thickness, *Bulletin of the Polish Academy of Science, Technical Sciences* 20 (1972) 229–234.
[4] V.B. Tungikar, K.M. Rao, Three-dimensional exact solution of thermal stresses in rectangular composite laminate, *Composite Structures* 27 (1994) 419–430.
[5] M. Savoia, J.N. Reddy, Three-dimensional thermal analysis of laminated composite plates, *International Journal of Solids and Structures* 32 (1995) 593–608.
[6] E.K. Hill, D.M. Egle, The forced vibrational response of a rectangular parallelepiped with rigid lubricated boundaries, *Journal of Sound and Vibration* 80 (1982) 61–69.
[7] H.A. Sosa, On the modelling of piezoelectric laminated structures, *Mechanics Research Communications* 19 (1992) 541–546.
[8] P. Heyliger, Static behaviour of laminated elastic/piezoelectric plates, *AIAA Journal* 32 (1994) 2481–2484.
[9] P. Heyliger, Exact solution for simply supported laminated piezoelectric plates, *Journal of Applied Mechanics* 64 (1997) 299–306.
[10] P. Bisegna, F. Maceri, An exact three-dimensional solution for simply supported rectangular piezoelectric plates, *Journal of Applied Mechanics* 63 (1996) 628–638.

[11] J.S. Lee, L.Z. Jiang, Exact electroelastic analysis of piezoelectric laminae via state space approach, *International Journal of Solids and Structures* 33 (1996) 977–990.
[12] S.S. Vel, R.C. Batra, Exact solution for rectangular sandwich plates with embedded piezoelectric shear actuators, *AIAA Journal* 39 (2001) 1363–1373.
[13] Z.Q. Cheng, C.W. Lim, S. Kitpornchai, Three-dimensional exact solution for inhomogeneous and laminated piezoelectric plates, *International Journal of Engineering Science* 37 (1999) 1425–1439.
[14] S.S. Vel, R.C. Batra, Three-dimensional analytical solution for hybrid multilayered piezoelectric plates, *Journal of Applied Mechanics* 67 (2000) 558–567.
[15] S.S. Vel, R.C. Batra, Analysis of piezoelectric bimorphs and plates with segmented actuators, *Thin Walled Structures* 38 (2001) 23–44.
[16] K. Xu, A.K. Noor, Y.Y. Tang, Three-dimensional solutions for coupled thermoelectroelastic response of multilayered plates, *Computer Methods in Applied Mechanics and Engineering* 141 (1997) 125–139.
[17] C. Zhang, Y.K. Cheung, S. Di, N. Zhang, The exact solution of coupled thermoelectroelastic behavior of piezoelectric laminates, *Computers and Structures* 80 (2002) 1201–1212.
[18] P. Heyliger, D.A. Saravanos, Exact free-vibration analysis of laminated plates with embedded piezoelectric layers, *Journal of the Acoustical Society of America* 98 (1995) 1547–1557.
[19] R.C. Batra, X.Q. Liang, J.S. Yang, The vibration of a simply supported rectangular elastic plate due to piezoelectric actuators, *International Journal of Solids and Structures* 33 (1996) 1597–1618.
[20] S. Kapuria, P.C. Dumir, A. Ahmed, Exact 2D piezoelasticity solution of hybrid beam with damping under harmonic electromechanical load, Zeitschrift für Angewandte Mathematik und Mechanik 84 (2004) 391–402.
[21] J. Ye, *Laminated Composite Plates and Shells: 3D Modelling*, Springer, Berlin, 2003.
[22] A.K. Noor, W.S. Burton, Three-dimensional solutions for initially stressed structural sandwiches, *Journal of Engineering Mechanics* 120 (1994) 284–303.
[23] Y.Y. Tang, A.K. Noor, K. Xu, Assessment of computational models for thermoelectroelastic multilayered plates, *Computers and Structures* 61 (1996) 915–933.